Journal of Power Sources 231 (2013) 279–284

Contents lists available at SciVerse ScienceDirect

Journal of Power Sources

journal homepage: www.elsevier.com/locate/jpowsour

A_2MgMoO_6 (A = Sr,Ba) for use as sulfur tolerant anodes

T.G. Howell [a,*], C.P. Kuhnell [a], T.L. Reitz [a], A.M. Sukeshini [b], R.N. Singh [c]

[a] Aerospace Systems Directorate, Air Force Research Laboratories, WPAFB, OH 45433, USA
[b] University of Dayton Research Institute, Dayton, OH 45469, USA
[c] School of Material Science and Engineering, Oklahoma State University, Stillwater, OK 74078, USA

HIGHLIGHTS

► Sr_2MgMoO_6 and Ba_2MgMoO_6 were generated as sulfur tolerant anodes. ► Sr_2MgMoO_6 and Ba_2MgMoO_6 showed better sulfur tolerance than Ni/YSZ. ► Sr_2MgMoO_6 demonstrated stability in all environments for an anode material. ► Ba_2MgMoO_6 formed impurities when fired in air 1300 °C and in 100 ppm H_2S at 800 °C. ► EDAX experiments showed evidence of sulfur accumulation in the LDC buffer layer.

ARTICLE INFO

Article history:
Received 20 September 2012
Received in revised form
10 December 2012
Accepted 1 January 2013
Available online 10 January 2013

Keywords:
Solid oxide fuel cells
Double perovskite
Sulfur tolerant anode
Sol–gel synthesis
Sr_2MgMoO_6
Ba_2MgMoO_6

ABSTRACT

The objective of this effort is to explore the substitution of the A-site in an A_2MgMoO_6 perovskite with Sr and Ba to improve the sulfur tolerance of solid oxide fuel cells (SOFCs). Perovskites have demonstrated superior sulfur tolerance but lack the high conductivity and catalytic activity of Ni/YSZ cermets. Sr_2MgMoO_6, a double perovskite, has been suggested as a material of interest because of its relatively high conductivity and catalytic potential. This study summarizes the synthesis of A_2MgMoO_6 (A = Sr,Ba) through sol–gel methods. The conductivity of the two samples was measured from thin pressed disks. Electrochemical performance of the specimens was performed by pasting the material onto an LSGM disk and stability was measured in sulfurous H_2 (140 ppm H_2S). Both SMMO and BMMO demonstrated superior stability when exposed to 140 ppm of H_2S as compared to Ni/YSZ, but did exhibit performance degradations due to sulfur accumulation in the buffer layer.

Published by Elsevier B.V.

1. Introduction

Solid oxide fuel cells (SOFCs) are high temperature fuel cells, normally operating at a temperature range of 650–1000 °C. SOFCs have several advantages over other types of fuel cells due to their relatively inexpensive material set, lower sensitivity to impurities in fuels and higher efficiencies [1]. Their high operating temperatures allow for the utilization of a variety of different fuels. Anodes tolerant to sulfur can allow for more direct utilization of hydrocarbon fuels while removing the need for costly desulfurization units to purify the fuel stream provided to the fuel cell. Conventional Ni/YSZ anodes are not compatible with sulfur due to nickel sulfide formation and subsequent breakdown of the active microstructure. Aviation fuels, in particular, can present a significant challenge because the sulfur concentration in these fuels can be as high as 0.3% by weight. Performance losses in SOFCs due to sulfur poisoning are associated with both physisorbed and chemisorbed sulfur species on the active nickel material [2]. The first cause is associated with the molecular adsorption of hydrogen sulfide (H_2S) at active surface sites resulting in an effective loss in available reaction sites for H_2/CO oxidation. This degradation mode is partially recoverable when H_2S is removed [3–7]. A second deactivation pathway occurs after the adsorption of sulfur onto a metal surface site and results in the subsequent sulfidation of that site to form metal sulfides. Blockage of active sites on the Ni surface is reversible when the adsorbed sulfur on a Ni surface is exposed to a pure H_2 fuel stream. However, sulfide formations have shown to be stable and exhibit little to no reversibility [8]. These metal sulfides often have a far lower melting temperature compared to the pure metal surface which results in a breakdown and rearrangement of the microstructure of the anode cermet. The rearrangement of the microstructure is not beneficial due to the decrease in porosity and increase in tortuosity. In the case of Ni/YSZ anodes,

* Corresponding author. Aerospace Systems Directorate, Air Force Research Laboratories, 1950 Fifth Street Building 18, WPAFB, OH 45433, USA. Tel.: +1 937 255 4226.
E-mail address: thomas.howell@wpafb.af.mil (T.G. Howell).

0378-7753/$ – see front matter Published by Elsevier B.V.
http://dx.doi.org/10.1016/j.jpowsour.2013.01.004

nickel sulfides are observed to melt below the standard operating temperature. As such, these conventional anode materials are rapidly poisoned due to the reactions of Ni and H_2S. A sulfidation degradation reaction for Ni anodes is shown below [2].

$$3Ni + 2H_2S \leftrightarrow Ni_3S_2 + 2H_2$$

Ni anodes have been observed to exhibit permanent degradation when exposed to 2 ppm of H_2S at 1000 °C, while for lower temperatures of 900 °C and 750 °C, permanent degradation has been observed with 0.5 ppm and 0.05 ppm, respectively. Deactivation of Ni anodes has been shown to increase with decreasing temperatures [9]. The poisoning becomes irreversible at low temperatures due to the thermodynamically stable adsorption of sulfur onto the Ni surface, and the resulting Ni_3S_2 formation [3]. As such, alternatives to Ni-based cermet anodes are a fervent area of research.

The objective of this effort is to explore the substitution of the A-site in an A_2MgMoO_6 perovskite with Sr and Ba to improve the sulfur tolerance of SOFCs. Perovskite materials are of interest as potential anode materials because they exhibit tailorable electrical conductivity and have demonstrated tolerance to sulfur and carbon depositions. Perovskite materials exhibit a chemical composition of ABO_3 where A-site dopants are commonly alkaline earth metals with an oxidation state of +2 while the B-site dopants are typically transition metals with an oxidation state of +4. A multitude of perovskites have been previously studied which include $La_{0.75}Sr_{0.25}Cr_{1-x}Mn_xO_3$, $La_{0.9}Sr_{0.1}Ga_{0.8}Cr_{0.2}O_3$, $LaCr_{0.9}Ti_{0.1}O_3$, $Y_{0.9}Ca_{0.1}FeO_3$, $SrCo_{0.8}Fe_{0.2}O_3$, $La_{0.9}Sr_{0.1}Ga_{0.8}Cr_{0.2}O_3$, $BaCe_{0.8}Y_{0.2}O_3$, $La_xSr_{1-x}VO_3$ and doped $SrTiO_3$ [10,12–15]. Certain perovskite formulations of $La_xSr_{1-x}Cr_{1-y}Mn_yO_3$ have shown to be resistance to sulfur exposure at levels as high as 10% H_2S [10]. Other ABO_3-type perovskites have demonstrated comparable sulfur tolerance but lack the high conductivity and catalytic activity of Ni/YSZ cermets [11]. Therefore, in order for these materials to be viable as fuel cell anodes, increases in their conductivity and catalytic performance are required.

Perovskite materials can be tailored for either n or p-type conductivity through selective doping of either A or B sites [16]. For example, oxide ion conductivity can be increased by selective doping of the A site with an element of a lower oxidation state resulting in an increase in charge carrier holes (p-type conduction) [16]. Furthermore, oxygen vacancies can be increased through partial reduction of the B-site from either B^{+4} to B^{+3}, or B^{+3} to B^{+2}, depending upon viable valence states of the B-site species. When a higher oxidation state is used as the A-site dopant, n-type conduction can be induced but can also promote p-type conduction as the B-site atom reduces to balance the A-site oxidation for molecular electroneutrality. A critical factor in promoting enhanced oxide ion mobility is the formation of a large number of oxygen vacancies in the perovskite structure. Oxygen vacancy concentration can be described as the sum of doping and reduction induced vacancies as shown in Equation (1) [16].

$$x = a/2 + \delta \tag{1}$$

Doping induced vacancies are described as the quantity of A^{+2} atoms which are substituted for A^{3+} on the A-site and are represented in Equation (1) by the term $a/2$ where "a" represents the substitution number of A^{+2} for A^{+3}. The second term, δ, is a function of oxygen partial pressure and varies with the oxidation state of the B-site. Electronic conductivity can also be shown to be dependent on the oxygen partial pressure. It has been shown previously for a variety of perovskite materials that B-site substitutions have a larger influence on the electronic conductivity as compared to A-site substitutions [16]. However, A-site substitution has been shown to play a larger role in ionic conductivity due to the introduction of a greater number of oxygen vacancies. In this study, the substitution of the A-site in an A_2MgMoO_6 perovskite with Ba and Sr was explored. It is envisioned that this study will elucidate the role of A-site substitution on perovskite electrochemical performance in high sulfur containing environments.

It has been shown that while doping of A and B sites can provide a favorable conductivity enhancement, excessive inclusion of dopants into the perovskite structure can be detrimental in terms of morphological integrity [17]. Incorporation of cations with different ionic radii into the crystal structure induces strain which must be distributed. Quantifying the extent of this strain as a function of dopant selection can be assessed based upon the relative ratios of the dopant ionic radii to the incumbent species. A formal expression of this, commonly referred to as the tolerance factor (t), describes the extent of strain induced into the perovskite structure due to doping of the A or B sites (Equation (2)).

$$t = \frac{(1-x)^*r_a + x^*r_a' + r_o}{\sqrt{2}^*\left((1-y)^*r_b + y^*r_b' + r_o\right)} \tag{2}$$

The tolerance factor can be determined by using Equation (2) for a doped double perovskite where x and y are the mole percent of dopant at the A and B sites, respectively; r_a is ionic radii of the A cation; r_a' is ionic radii of the A-site dopant; r_b is the ionic radii of the B cation; r_b' is the ionic radii of the B-site dopant and r_o is the ionic radii of oxygen anion [18].

A stable perovskite structure should fall in between tolerance factor values of 0.75 and 1, with 1 being an ideal cubic structure. When the tolerance factor is between 0.75 and 0.9, an orthorhombic crystal structure will generally occur. However, perovskites with a tolerance factor between 0.95 and 1.04 exhibit a cubic crystal structure [19]. The tolerance factor can be useful in predicting how the level of doping will affect material properties including electrical conductivity and catalytic activity. A highly defective structure can be required to improve electrical and ionic properties to a desirable value.

2. Experimental

2.1. Sample powder preparation

Samples of SMMO and BMMO were prepared via sol–gel synthesis. It is important, when using sol–gel synthesis, to ensure the molarities of the stock solutions used are correct due to the uncertain extent of hydration of the precursor material. This process involves dissolving precursor nitrates including $Sr(NO_3)_2$, $Mg(NO_3)_2$ and $(NH_4)_6Mo_7O_{24}$ into de-ionized water to generate stock solutions. Precise metal stoichiometry is required to get pure phase perovskite structures. Therefore, in the sol–gel synthesis, 10 mL of stock solutions were placed into a crucible to determine the correct molarity of the stock solutions. The crucible was placed in a furnace with a heating profile of 1 °C per minute to 300 °C, and was held at 300 °C for 2 h, then ramped at 1 °C per minute to 800 °C, and held at 800 °C for 2 h. This heating profile allowed the conversion of nitrates to oxides which was verified using thermogravimetric analysis (TGA) and X-ray diffraction (XRD). The molybdate stock solution was prepared similarly but was held at a lower temperature of 200 °C.

BMMO was prepared by using Mg stock solution, Mo stock solution and $Ba(NO_3)_2$. Nitrate solutions were added to a reaction flask and stirred vigorously using a stir bar. A mixture of equimolar citric acid and ethylene glycol was added as a chelating agent. The molar ratio was 1:1 citric acid to metal nitrates. Once the chelating agent was added, the solution was placed on a hot plate and stirred vigorously at 300 °C. The pH was adjusted using diluted nitric acid to maintain a pH between 1 and 2, which ensured that the reactants remained in solution. Once the solution was clear, the hot plate

temperature was increased to 400 °C and the solution was allowed to evaporate. Solution viscosity steadily increased during evaporation until a gel formed. This gel self-ignited, forming powder once the combustion reaction was finished. The same methodology was used to prepare SMMO except that ethylenediaminetetraacetic acid (EDTA) was used as the chelating agent. The powder was then pressed into pellets which were calcined for an additional 6 h at 800 °C. After initial calcinations, the pellet was re-ground using the shaker mill and re-pressed. The pellets were then annealed for 24 h at 1100 °C, followed by further heat treatment for 12 h at 1200 °C in 5% H_2. Annealing helps generate oxygen vacancies and removes impurities from the material. After annealing, the powder was reground using the shaker mill.

2.2. Characterization

Both materials were characterized to determine XRD phase purity with a Rigaku DMAX B RU200 X-ray diffractometer and Cu Kα radiation with a scan speed of two degrees per minute. The scans were performed in the 2θ range from 15° to 80°. Crystal structure and relevant phases were assigned using MDI-Jade software.

The conductivity of each material was tested employing a fully dense sintered disc which was fired at 1300 °C measuring 15 mm in diameter and 1.5 mm in thickness using electrochemical impedance spectroscopy (EIS). Pt paste (Heraeus) was applied to each side of the discs to serve as current collectors and fired at 1200 °C for 2 h. Silver wires were attached to the Pt electrodes using gold paste which was cured at 150 °C for 1 h. The stability of the materials was tested by pressing a pellet of 15 mm diameter by 1.5 mm. The coupon was then fired at 1300 °C for 2 h in air to ensure compatibility of the coupon with common electrolytes such as $La_{0.8}Sr_{0.2}Ga_{0.83}Mg_{0.17}O_{2.815}$ (LSGM). The pellet was then placed in a reducing environment for 400 h in hydrogen to ensure stability in relevant environments for prolonged periods. Then the pellets were exposed to 100 ppm of H_2S for 90 h to assess materials stability in high sulfur containing environments. After each test, X-ray diffraction patterns were generated to see if any structural changes could be observed in the materials.

The sulfur tolerance and electrochemical performance of the materials were tested by preparing an ink of the perovskite materials which are pasted onto $La_{0.4}Ce_{0.6}O_{1.8}$ (LDC) coated $La_{0.8}Sr_{0.2}Ga_{0.83}Mg_{0.17}O_{2.815}$ (LSGM) electrolyte discs. $La_{0.8}Sr_{0.2}MnO_{3-x}$ (LSM) was used as a counter electrode. LSGM was selected as the electrolyte for this study as it was deemed to be more compatible with Sr-based perovskites in that the potential formation of $SrZrO_3$ phases, common in YSZ, would be avoided [20]. Prior to use, the LSGM electrolyte disc was ground to approximately 500 μ using a diamond wheel. A 25 ± 5 μ buffer layer of LDC fired at 1200 °C for 2 h was used between the perovskite anode and LSGM electrolyte to prevent lanthanum diffusion from the electrolyte into the anode. A 25 ± 5 μ perovskite anode layer was pasted and fired at 1300 °C for 2 h in air. Gold paste was used to fix the silver wires onto the cell as a current collector. The cells were mounted on the end of an alumina tube using high temperature paste (Aremco Ultra-Temp 516). The cell test fixture was then placed into a split tube furnace and reduced for 8 h in 5% H_2. Dry hydrogen was used for all cell characterization experiments. The cells were then exposed to 140 ppm of H_2S in H_2 at 800 °C after which time they were polarized galvanostatically wherein the cell performance was monitored to determine the extent of degradation due to sulfur poisoning.

3. Results and discussion

In order to confirm the desired purity of the double perovskites was achieved, XRD experiments were performed on SMMO and BMMO (Figs. 1 and 2) prepared through sol–gel methods. The SMMO XRD plot analyzed with MDI Jade 5 software showed monoclinic phase with space group P2 while BMMO was triclinic with space group P1. The lattice parameters for SMMO (Table 1) and BMMO (Table 2) are listed for the all the environments and firing temperatures. It is evident from the XRD data that the samples prepared were X-ray phase pure.

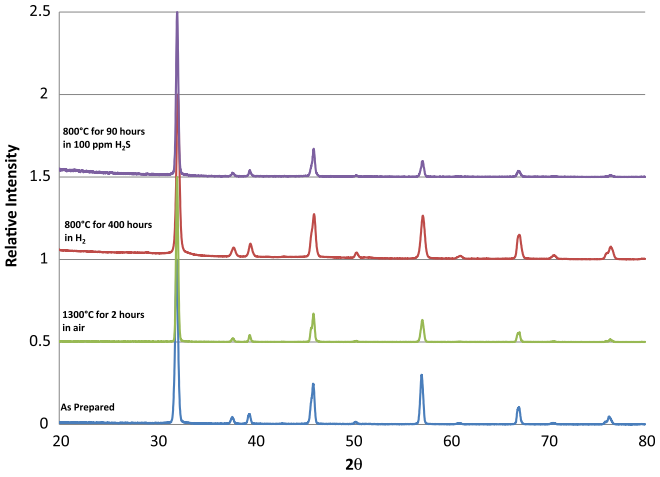

Fig. 1. SMMO diffraction pattern for various environments.

To assess the stability of A-site substitution in an A_2MgMoO_6 perovskite with Sr and Ba cations, these materials were subjected to different heat treatment steps in an attempt to simulate the environments common to SOFC production and operation. The first experiment was to assess material stability in an oxidizing environment as observed when firing the anode onto the electrolyte substrate. The second experiment sought to further examine structural stability when the material is exposed to hydrogen at 800 °C for 400 h which is representative of anode operational environments. The final step was to characterize sulfur tolerance by exposing the pellet to 100 ppm H_2S in H_2 at 800 °C for 90 h. From Fig. 1, it can be observed that the SMMO is structurally stable under all the treatment conditions and there was no evidence suggesting a breakdown in the structure of the parent phase.

BMMO was exposed to the same series of tests as SMMO but overall stability was less than that observed for SMMO, especially when exposed to sulfur. In Fig. 2 it is shown that evidence of this phase instability is apparent from the formation of $BaMoO_4$ species

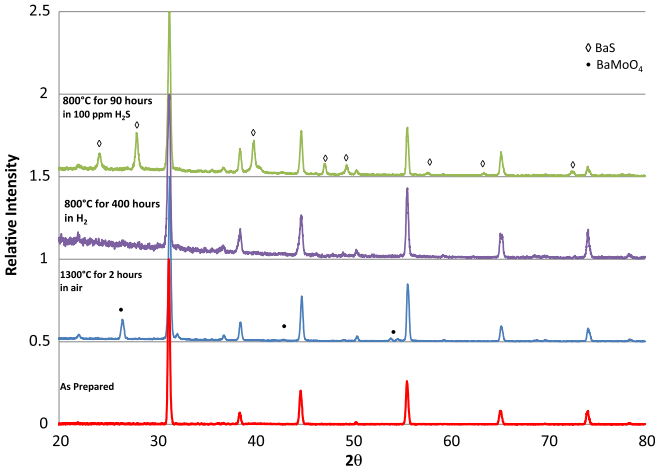

Fig. 2. BMMO diffraction pattern for various environments.

Table 1
SMMO lattice parameters.

Material	Sr_2MgMoO_6	Sr_2MgMoO_6	Sr_2MgMoO_6	Sr_2MgMoO_6
Environment	After processing	800 °C H_2	1300 °C in air	800 °C 100 ppm H_2S/H_2
a (Å)	5.949	5.951	5.970	6.021
b (Å)	7.887	7.884	7.880	7.843
c (Å)	5.569	5.566	5.564	5.555
β (°)	89.6	89.6	89.4	89.3
V (Å^3)	261.274	261.13	261.686	262.329

when BMMO is exposed to air at 1300 °C. Upon subsequent exposure to hydrogen for 400 h at 800 °C, the $BaMoO_4$ impurity is observed to disappear and a pure BMMO structure is re-obtained. $BaMoO_4$, when exposed to hydrogen, will remain stable until 920 °C whereupon reduction to $BaMoO_3$ has been observed to occur [21]. When a pellet of BMMO fired in air at 1300 °C is exposed to 100 ppm H_2S treatment at 800 °C, the $BaMoO_4$ phase does not reappear but peaks attributed to the formation of BaS appear. The limited phase stability of BMMO in air and H_2S/H_2 suggests that it may not be a viable candidate for SOFC anodes.

In order to assess the impact on material conductivity of A-site substitution in an A_2MgMoO_6 perovskite with Sr and Ba, an experiment was performed where varying Sr and Ba concentrations were substituted into the A-site of the perovskite structure. Barium was selected as the dopant because the ionic radii (1.61 Å) resulted in a calculated tolerance factor of 1.036 for BMMO when compared to SMMO, which has an ionic radii of 1.44 Å and a calculated tolerance factor of 0.978. The tolerance factor for $BaSrMgMoO_6$, a bi-substituted material synthesized for comparison as an intermediate formulation, was calculated to be 1.00. It was concluded in a study of single perovskites that the ideal tolerance factor is 0.96 to optimize the electrical conductivity [17]. As such, it is anticipated that Ba-substituted double perovskites would exhibit lower conductivity and electrochemical activity than Sr-substituted double perovskites. As is evident from the conductivity results presented in Table 3, tolerance factors closer to 1 exhibit higher conductivity values. It has been suggested in previous studies that the formation of $SrMoO_4$ impurities in SMMO when fired in air may favorably impact conductivity once reduced due to the formation of the single perovskite $SrMoO_3$ which has been observed to be more electrically conductive than SMMO [22]. In this study, however, no evidence of $SrMoO_4$ was observed unlike that observed in the BMMO. This impurity is likely responsible for the higher measured conductivity values of the BMMO material.

Mixed ionic and electronically conductive materials generally exhibit activation energies in the region of 0.1–1 eV. However values closer to 0.1 eV are thought to be indicative primarily of electron hopping while those closer to 1.0 eV to be oxide ion mobility [23]. All materials studies in this work exhibit activation energies in the region of 0.03–0.44 eV suggesting a greater proportion of the electron conductivity than ionic.

Table 2
BMMO lattice parameters.

Material	Ba_2MgMoO_6	Ba_2MgMoO_6	Ba_2MgMoO_6	Ba_2MgMoO_6
Environment	After processing	800 °C H_2	1300 °C in air	800 °C 100 ppm H_2S/H_2
a (Å)	5.654	5.663	5.662	5.705
b (Å)	5.447	5.500	5.500	5.396
c (Å)	7.964	7.993	7.990	8.018
α (°)	89.48	88.88	88.87	88.89
β (°)	90.54	90.91	90.9	90.62
γ (°)	91.25	91.11	91.13	92.33
V (Å^3)	245.194	248.814	248.665	246.561

Table 3
Conductivity of Ba doped SMMO.

Sample	*σ* (S cm^{-1})	Ea (eV)	Tolerance factor
Sr_2MgMoO_6	0.46	0.44	0.978
$BaSrMgMoO_6$	5.32	0.22	1.002
Ba_2MgMoO_6	3.92	0.03	1.036

As discussed previously, the conductivity of the materials was examined over 90 h in a 100 ppm H_2S environment at 800 °C to examine how the anode material would operate in a sulfur rich environment. The results presented in Fig. 3 illustrates that the BMMO continues to decrease in conductivity with time when exposed to 100 ppm H_2S/H_2 environments. This data is consistent with that presented in Fig. 2, suggesting BaS formation has a detrimental impact on the material bulk conductivity. Conversely, SMMO initially decreased in conductivity and then stabilized after 70 h. This data agrees with the XRD studies shown in Fig. 1 wherein no sulfides are formed in the SMMO material upon exposure to H_2S. To examine how these materials perform as SOFC anodes, SMMO and BMMO were deposited onto an LDC/LSGM/LSM cell and the performance of these cells were evaluated galvanostatically at 50 mA and the data is presented as Fig. 4. A nearly constant deactivation rate of 1.5 mV h^{-1} was observed for the SMMO full cell when exposed to both pure hydrogen and 140 ppm H_2S/H_2 environments. This performance decrease is considered negligible when compared with conventional YSZ/NiO cells which exhibit far greater deactivation rates. BMMO based cells, by contrast, exhibit an improvement of 0.5 mV h^{-1} independent of whether H_2 or H_2S/H_2 environment. While deactivation rates observed for both material sets studied in this work were significantly better than the conventional YSZ/NiO anode material, differences in the deactivation modes are suspected for SMMO and BMMO. The SMMO anode degradation would seem to suggest that sulfur adsorption and blocking of active sites is still a factor, though significantly less than Ni-based anodes. Given that no evidence of SrS has been observed in this study the exact cause of the cell's loss in performance is unclear; speculation might suggest accumulation of sulfur in other active regions within the anode. Therefore, even though some evidence of BaS was observed during the material stability evaluations shown previously (Fig. 2), relative stability of the cell appears to be observed for the limited time of this test. It can be speculated that this relative stability is associated with the $BaMoO_4$ reducing into the more conductive $BaMoO_3$ when subjected to prolonged H_2

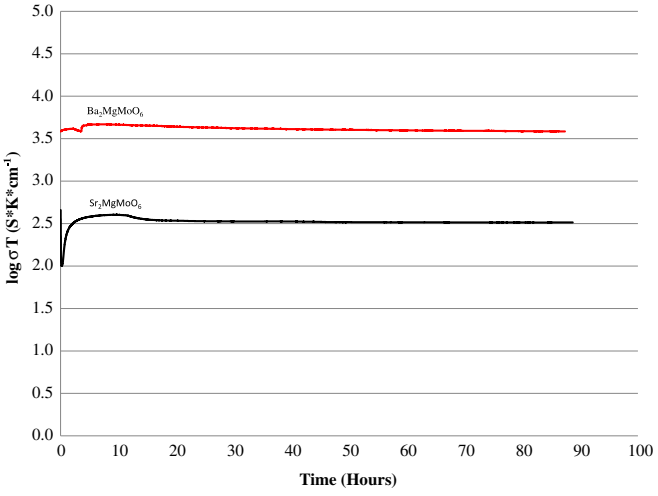

Fig. 3. Pellets of SMMO and BMMO exposed to 100 ppm H_2S.

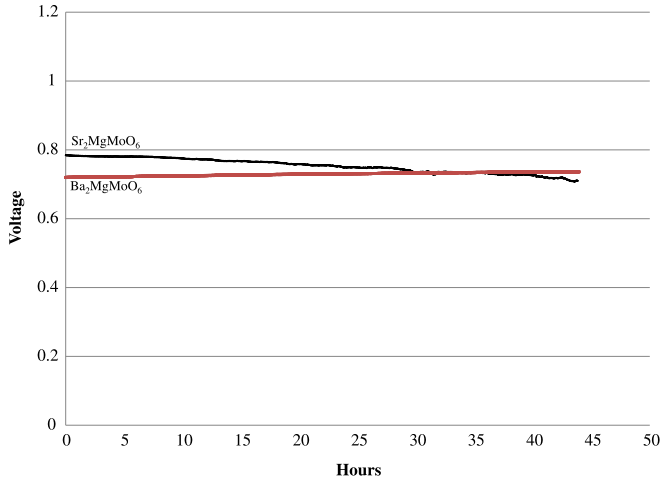

Fig. 4. Long term sulfur in 140 ppm.

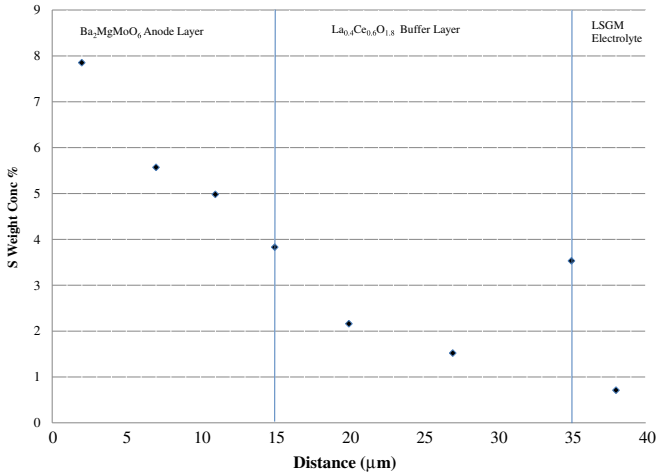

Fig. 6. EDX analysis of BMMO for presence of sulfur in various layers.

treatment, resulting in an anode conductivity increase which may mask some of the degradation associated with the formation of BaS.

The exact role of the A_2MgMoO_6 anode material in the A_2MgMoO_6/LDC/LSGM/LSM layered configuration remains unclear. In order to understand the degradation of A_2MgMoO_6, an experiment was conducted to examine the sulfur adsorption characteristics of each material within an LDC-buffered SMMO/LSGM/LSM cell with prolonged exposure to H_2S. The experiment was conducted by taking a complete SMMO/LDC/LSGM/LSM and a BMMO/LDC/LSGM/LSM cell as described previously and exposing it to 140 ppm of H_2S under galvanostatic polarization. Once this pretreatment was complete, the cell was removed and the fracture cross section was imaged via SEM and elemental analysis was obtained by EDAX. For an SMMO cell with an LDC buffer layer, no evidence of sulfidation or physical absorption of sulfur within the SMMO anode layer was observed based upon post-exposure analysis by EDAX and XRD. However, the data from Fig. 5 appears to suggest sulfur accumulations within the LDC layer which suggests irreversible H_2S adsorption affinity. When analyzing the SMMO cell via EDAX, the highest sulfur concentrations by weight percent were present in the LDC buffer layer, while the anode and electrolyte showed negligible sulfur accumulation. This sulfur accumulation suggests that sulfur adsorption and blocking of active sites will play a role in the overall stability of a cell. For a BMMO cell with an LDC buffer layer there is an evidence of sulfidation occurring within the anode layer based on the post-exposure analysis by EDAX and XRD. Fig. 6 shows the accumulation of sulfur in the BMMO anode due to the sulfidation that occurs as a result of BaS formation. It is suspected that the sulfur accumulations in the LDC layer of the BMMO cell is less than that observed in the SMMO cell due to the barium sulfidation that is occurring in the anode layer.

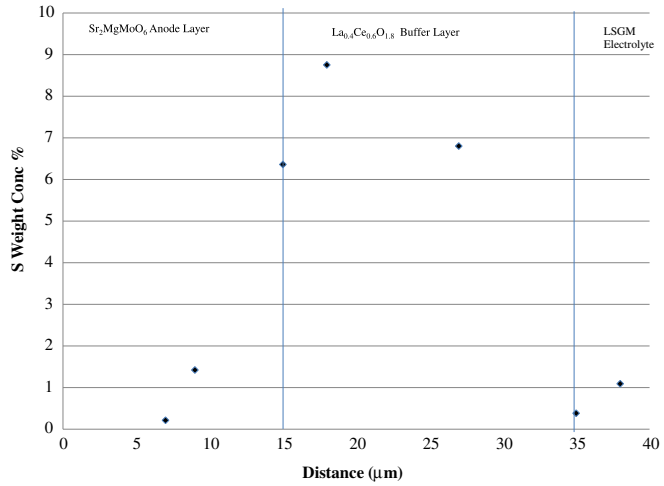

Fig. 5. EDX analysis of SMMO for presence of sulfur in various layers.

4. Conclusions

The goal of this effort was to explore the substitution of the A-site in an A_2MgMoO_6 perovskite with Sr and Ba to improve the sulfur tolerance of solid oxide fuel cells (SOFCs). SMMO was demonstrated to be stable in various environments common for an anode material. While BMMO was shown to be stable in an anode environment, partial decomposition of the perovskite structure was observed when fired in an oxidizing environment. Primary phase impurities were $BaMoO_4$ under oxidizing conditions and BaS when it is exposed to H_2S containing hydrogen streams. Both BMMO and SMMO demonstrated superior stability relative to a conventional Ni/YSZ cermet when exposed to high sulfur concentrations in the anode fuel stream; however, some degradation in performance was observed. For the BMMO sample, a slight voltage increase occurred, attributed to the formation of $BaMoO_4$ forming $BaMoO_3$ which will improve the overall conductivity and outweigh the decrease in conductivity from BaS. For the SMMO sample, the decrease in performance is thought to be associated with the accumulation of sulfur in the LDC buffer layer as evident from EDAX experiments. Through a series of A-site dopant experiments, the tolerance factor was lowered from 1.036 to 0.977 and the conductivity was observed to be the highest at a tolerance factor of 1 yielding a conductivity of 5.32 S cm^{-1} for $BaSrMgMoO_6$. BMMO has demonstrated to have a higher conductivity than SMMO but not the stability in a 100 ppm H_2S.

References

[1] J. Goodenough, Y.H. Huang, J. Power Sources 173 (2007) 1–10.
[2] M. Gong, X. Liu, J. Trembly, C. Johnson, J. Power Sources 168 (2007) 289–298.
[3] G. Offer, J. Mermelstein, E. Brightman, N. Brandon, J. Am. Ceram. Soc. 92 (2009) 763–780.
[4] N. Galea, E. Kadantsev, T. Ziegler, J. Phys. Chem. C 111 (2007) 14457–14468.
[5] E. Albenze, A. Shamsi, Surf. Sci. 600 (2006) 3202–3216.
[6] Y. Choi, C. Compson, M. Lin, M. Liu, Chem. Phys. Lett. 421 (2006) 179–183.
[7] J. Dong, Z. Cheng, S. Zha, M. Liu, J. Power Sources 156 (2006) 461–465.
[8] C. Bartholomew, Appl. Catal. A: Gen. 212 (2001) 17–60.
[9] Y. Matsuzaki, I. Yasuda, Solid State Ionics 132 (2000) 261–269.
[10] S. Zha, P. Tsang, Z. Cheng, M. Liu, J. Solid State Chem. 178 (2005) 1844–1850.

[11] C. Sun, U. Stimming, J. Power Sources 171 (2007) 247–260.
[12] S. Wang, M. Liu, J. Winnick, J. Solid State Chem. 5 (2001) 188–195.
[13] A. Tomita, K. Tsunekawa, T. Hibino, S. Teranishi, Y. Tachi, M. Sano, Solid State Ionics 177 (2006) 2951–2956.
[14] L. Aguilar, S. Zha, Z. Cheng, J. Winnick, M. Liu, J. Power Sources 135 (2004) 17–24.
[15] O. Marina, N. Canfield, J. Stevenson, Solid State Ionics 149 (2002) 21–28.
[16] H. Ullman, N. Trofimenko, F. Tietz, D. Stover, A. Ahmad-Khanlou, Solid State Ionics 138 (2000) 79–90.
[17] H. Hayashi, H. Inaba, M. Matsuyama, N.G. Lan, M. Dokiya, H. Tagawa, Solid State Ionics 122 (1999) 1–15.
[18] H. Ullman, N. Trofimenko, J. Alloys Compd 316 (2001) 153–158.
[19] A. Sammells, R. Cook, J. White, J. Osborne, R. MacDuff, Solid State Ionics 52 (1992) 111–123.
[20] K. Huang, J. Wan, J. Goodenough, J. Electrochem. Soc. 148 (2001) A788–A794.
[21] V. Nassif, R.E. Carbonio, J. Solid State Chem. 146 (1999) 266–270.
[22] S. Vasala, H. Yamauchi, M. Karppinen, J. Solid State Chem. 184 (2011) 1312–1317.
[23] X. Dong, P. Gardner, T.L. Reitz, F. Chen, in: P. Singh, N.P. Bansal (Eds.), Advances in Solid Oxide Fuel Cells VI: Ceramic Engineering and Science Proc. (CESP), vol. 31 (issue 4), Wiley, 2010, pp. 31–41.